Analysis and Control of a Modular Multilevel Cascaded Converter-based Unified Power Flow Controller

Han Huang, *Member, IEEE*, L. Zhang, *Senior Member, IEEE*, O.J.K. Oghorada and Mingxuan Mao, *Member, IEEE*

Abstract*--This paper presents a novel configuration for a unified power flow controller (UPFC) comprising a modular multilevel cascaded converter (MMCC) with a full-bridge inverter. The MMCC has one end of each phase-leg shunt-connected to the transmission line. The other end connects in parallel to the primary terminals of a series line transformer, and the ac output terminals of a full-bridge dc-ac inverter. The submodules in the MMCC are full-bridge flying capacitor converters. This UPFC is compared to another type of MMCC-UPFC which uses double-star configuration, and submodules of half-bridge chopper type; this is referred to as the Double Star Chopper Cells UPFC (DSCC-UPFC). The comparison is in terms of footprint, cost and performance. The new topology is lighter, more efficient and cheaper than the DSCC. Its operating principle and control scheme, which combines the regulation of voltage and of transmission line power flow, are presented. Simulation studies for the proposed MMCC-UPFC realising power flow control in a dual voltage sourced power network are presented and show good performance under varying operation conditions. The paper also evaluates the power control margins of this device.

***Index Terms*—Modular multilevel converters; Flexible AC transmission systems; Power control.**

I. Introduction

Recent advances in power electronics have encouraged progress in Flexible AC Transmission Systems (FACTS), with sophisticated configurations and control techniques for managing power flow in large utility networks. These devices offer power quality improvement, highly flexible control and fault tolerance in power systems. Transmission loss, power transfer capability and reliability may all be improved. Amongst all the FACTS devices, the Unified Power Flow Controller (UPFC) is the most versatile [1]. It can simultaneously realise voltage regulation, line impedance compensation and phase angle adjustment, and harmonic reduction; it offers independent control of real and reactive power flows along the compensated transmission lines and increases power transfer stability margins [2, 3].

The conventional UPFC configuration is a combination of two voltage source converters (VSCs), connected 'back-to-back' through a common dc-link. One of the VSCs is connected in parallel with the transmission line through a voltage step-down transformer. The other is connected in series with the transmission line through a series transformer. The former performs functions of regulating voltages of the point of common coupling (PCC), giving real power exchanges between the two VSCs, and maintaining the dc-link capacitor voltage at its nominal level. The series VSC controls real and reactive power flows along the transmission line by injecting a 4-quadrant controllable ac voltage to the primary side of a transformer. As it can be seen, both the dc-link bus and interfacing transformers cannot be neglected as the former offers real power supplement for the VSC_2 from VSC_1, and the latter provides voltage matching and galvanic isolation between the device and transmission line. However, the requirement of a bulky transformer increases cost, losses and footprint [4], as well as reduces dynamic response speed. To eliminate the disadvantages several alternative UPFC topologies have been investigated [5-7], but they still have drawbacks such as requiring bulky transformers on both sides.

Within the last decade, the modular multilevel converters (MMC) have made a significant contribution to the medium and high voltage power system due to its modularity, reliability and high power density [8, 9], hence the MMC-based UPFC applications have also gained attention [10-13]. In the recent published literatures, authors have contributed to the MMC-UPFC modelling, its interaction with power system and control strategies under abnormal grid conditions. In [14] A. M. Vural et al presented a detailed simulation model of the MMC-UPFC. The harmonic influence in grid caused by this type of devices is studied in [15]. Also, in order to analyse the power system stability and low-frequency oscillation characteristics, a small-signal model of the MMC-UPFC is proposed [16]. In this paper the authors also listed existing six UPFC projects including three MMC based structures around the world. Under unbalanced grid conditions, a symmetric component control is investigated to balance the transmission line current by using the MMC-UPFC [17]. It also presented a voltage limit control to protect the device from over-modulation. Recently Yang et al introduced a model predictive control scheme for the MMC-UPFC under unbalanced conditions [18]. The paper claimed that UPFC can be controlled flexibly by regulating the reference power factor in a cost function.

Most MMC-UPFCs reported in the literature are based on the Double Star Chopper Cells (DSCC) as shown in Fig. 1. This is configured by 3-phase top and bottom arms connected respective to the +ve and –ve dc-buses while each arm consists of equal number of chopper (half bridge) submodules in chain link and filter inductor. This configuration is more expensive and complicated to control than the one based on Single Star Bridge Cells (SSBC)[19]. An alternative nine-arm MMC-UPFC topology thus is proposed in [20], which can reduce the

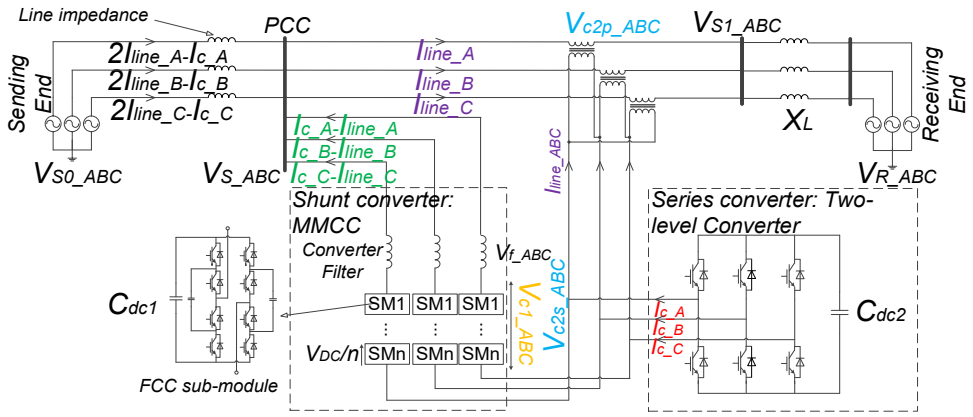

Fig. 2. A 3-phase distribution system with novel MMCC-UPFC circuit diagram

number of required submodules by 25% and inductors by 50%. However, it still requires large footprint and cost since the submodules are based on half bridge circuit.

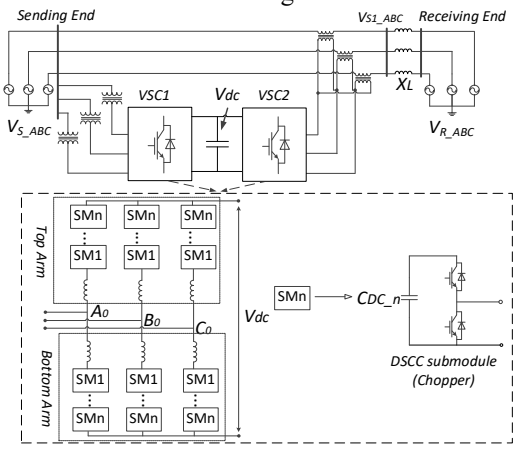

Fig. 1. A simplified distribution system with DSCC-UPFC

This paper proposes a single star Modular Multilevel Cascaded Converter-based UPFC (MMCC-UPFC). Unlike the conventional MMC-UPFC structure which is based on two DSCCs connecting back-to-back via a common dc-link, in this configuration the two VSCs are linked on the ac side directly. Section II of this paper describes the MMCC-UPFC system structure and operating principle; Section III compares the novel configuration with the DSCC-UPFC topology from different aspects in a real world environment; The control strategies of the shunt MMCC and series converter of the UPFC are given in Section IV. Simulation studies are discussed in Section V showing the effectiveness and controllability of the device. Finally, Section VI assesses the power transfer margin of a transmission line that the UPFC can improve and as well as its operation range.

II. MMFCC-BASED UPFC SYSTEM DESCRIPTION

A. Novel MMCC-UPFC circuit with 3-phase distribution system

The proposed structure of a grid-connected MMCC-UPFC is shown in Fig. 2. V_{S0_ABC} and V_{R_ABC} represent respectively the sending and receiving end voltages of a 3-phase balanced network linked by a transmission line. An MMCC is shunt-connected to the Point of Common Coupling (PCC) as VSC_1, which contains multiple submodules (SM) in each phase so that it can meet the distribution voltage level requirement. The SMs could be either full H-bridge (HB) or any other converter topologies, here the 3-level Flying capacitor converter (FCC) is used. Hence each SM consists of eight transistors, three capacitors; an outer one C_{dc1}, and two inner flying capacitors. Each SM can synthesis five voltage levels; $\pm V_{dc}$, $\pm 0.75V_{dc}$, $\pm 0.5V_{dc}$, $\pm 0.25V_{dc}$ and 0 Volt. The number of chained SMs may vary according to the transmission line voltage rating and the dc capacitor voltage per module. On the series side of the UPFC a 2-level bridge converter is connected to the transmission line via a series transformer. Its 3 phases' ac sides are connected to a three-phase transformer whose primary side windings are connected in series with the transmission line. This UPFC structure has the following advantages:

- Full modularity and flexibility in adjusting voltage levels since each SM can be individually controlled and bypassed when fault occurs.
- The requirement of total SM number and control complexity is reduced.
- It is shunt connected to the transmission line through an inductor filter, thus no bulky transformer at the shunt section is required.
- There are no shared capacitors between the shunt MMCC and the series VSC, but each SM has its own capacitors.

B. Operating principle

The UPFC equivalent circuit and its voltage and current phasor diagram are illustrated in Fig. 3. The series transformer is a Y-Δ connection and a desired $\sqrt{3}V_{c2s}\angle(\delta - 30°)$ is generated at the converter side. This will be converted to $V_{c2p}\angle\delta$ of 30º phase angle leading at the transmission line side. The current flowing out from the series converter is $\overrightarrow{I_c}$, which should be controlled in quadrature with its voltage $\overrightarrow{V_{c2s}}$ and thus entirely reactive. Moreover, the shunt converter voltage is in between with the PCC voltage and series

converter voltage, thus can be derived as $(\overrightarrow{V_s} - \overrightarrow{V_{c2s}})$, which is equivalent to the MMCC's voltage $\overrightarrow{V_{c1}}$ plus inductor filter voltage drop $\overrightarrow{V_f}$. The current generated by the MMCC is according to the series converter and transmission line current as $(\overrightarrow{I_c} - \overrightarrow{I_{line}})$, which is also perpendicular with its voltage $\overrightarrow{V_{c1}}$ and therefore entirely reactive.

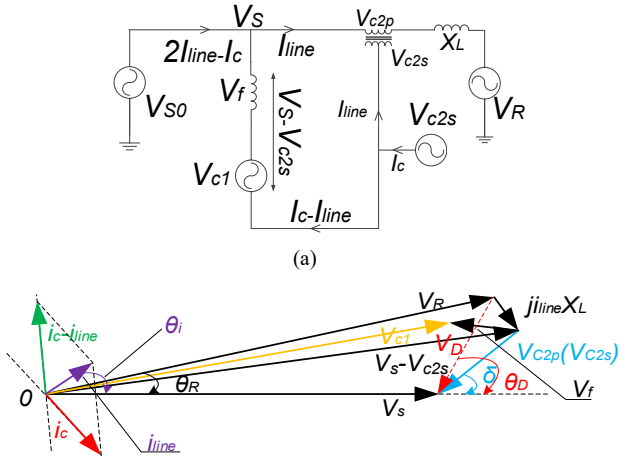

Fig. 3. (a) MMCC-UPFC equivalent circuit; (b) its voltage and current phasor diagram

The current flowing through the MMCC plays an important role in controlling both shunt submodules and series converter dc capacitor voltages, as it controls not only PCC voltage regulation, but also the two converters' current in quadrature with their voltages. However, losses in the devices exist which consume real power, hence an additional control to compensate losses of real power is required for the MMCC. It is expected that it can generate exact current for the purpose of zero active power exchange between the two converters. The details of control strategy are introduced in the Section IV.

III. Comparing with the DSCC-UPFC Configuration

The key criteria to compare the novel single star MMCC-UPFC configuration and SMs with the DSCC-UPFC are the footprint, cost and performance under the same voltage rating. Fig. 4 shows the general arrangement of an MMCC single arm in high voltage platform [21, 22]. As well-known, one half-bridge SM circuit essentially consists of one capacitor, one switch module (in pair) and gate electronics [23]. The size percentages of each components based on it are listed in Table I. Similarly, one H-bridge contains one capacitor, two switch modules and gate electronics; one FCC bridge includes three capacitors, four switch modules and gate electronics, respectively. Therefore, the H-bridge and FCC bridge cells can be regarded as 140% and 240% X_{sm} (depth) of the half-bridge circuit, as shown in Fig. 4. Besides, there are also insulators between each two layers to provide insulations.

Assume that the UPFC is installed in an 11 kV distribution system, Table I gives a list of the key components typically used for this voltage level [24]. The comparisons are as follows:

TABLE I
KEY COMPONENTS FOR MMC HALF-BRIDGE SUBMODULE ANALYSIS

Component	*Manufacture Part No.*	*Rating*	*Cost (£)*	*Size*
IGBT Switch Module	Infineon IKW30N60TFKSA1	600V, 30A	7.5 (pair)	20% of half-bridge submodule
Capacitor	Nichicon LGL2G561MELB40	400V, 560μF	10.54	Typical 50%-60% of half-bridge submodule
Gate Electronics	Microsemi ProASIC3 FPGA Board	Only key parts are considered	6.75	20% of half-bridge submodule
	LEM LV 25-P Voltage Transducer		59.93	
	Gate drive & Isolation (ACPL-332J; MEV1S0515SC)		12.85	
Heat Sink	Fisher elektronics SK105/105SA	R_{th}=2K/W	6.58	-

Footprint: The MMCC footprint calculation for each phase is based on the height and width of the platform, as shown in Fig. 4. X_{sm} is the depth (d) of the platform and X is the total width (w) which is according to the SM numbers per tier n_{sm}, while Y is the total height (h) based on the height of each SM, Y_{sm}; the insulation clearance gap distance between tiers, Y_{cd}, and the number of tiers n_t. n_t is limited by the local building height and may be restricted by planning regulations, hence set as fixed values of 7 for all cases in this paper [21].

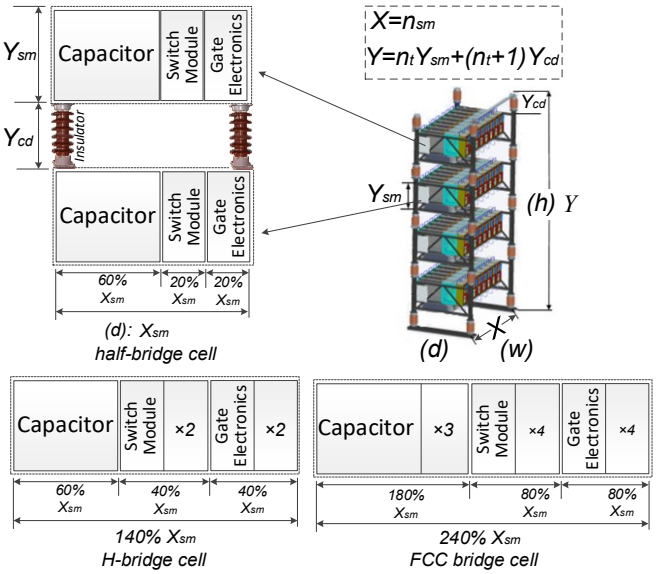

Fig. 4. MMCC single phase footprint

Therefore, the footprint of this MMCC arm can be calculated as

$$XYX_{sm} = [n_t Y_{sm} + (n_t + 1)Y_{cd}]n_{sm}X_{sm} \quad (1)$$

where $Y_{cd} = \text{USCD} * \text{voltage rating}/n_t$, USCD is the unified specific creepage distance and specified as 3.5 cm/kV in IEC60185 [25]. Y_{sm} is based on a Heat Sink, and has the largest size of 20 cm, and X_{sm} is assumed to be three times of the height which equals to 60 cm. Hence, the 3-phase single star MMCC-UPFC and DSCC-UPFC footprint for an 11 kV level application can be calculated as Table II.

TABLE II
ESTIMATED FOOTPRINT COMPARISON OF PROPOSED UPFC AND DSCC-UPFC

	Single star based - UPFC				***DSCC -UPFC***	
	Shunt side	Series side	Shunt side	Series side	Shunt side	Series side
SM type	3-level h-bridge	Bridge converter	5-level flying capacitor	Bridge converter	2-level half bridge	2-level half bridge
SM Qty. per phase	28	1	14	1	112	112
Tiers No.(n_t)	7	1	7	1	7	7
***h*d*w* (m^3)**	**19.1**		**23.1**		**105.8**	

Cost: The overall cost is estimated according to the number of key components and their corresponding prices which are listed in Table I. It is worth mentioning that the component numbers are different not only because of the MMCC configurations, but also due to the calculation based on different SM types, as shown in Table III.

TABLE III
ESTIMATED COST COMPARISON OF PROPOSED UPFC AND DSCC-UPFC

	Single star based – UPFC				***DSCC -UPFC***	
	Shunt side	Series side	Shunt side	Series side	Shunt side	Series side
SM type	3-level h-bridge	Bridge converter	5-level flying capacitor	Bridge converter	2-level half bridge	2-level half bridge
No. of switch module	168	3	168	3	336	336
No. of capacitor	84	1	168	1	336	336
No. of FPGA	84	1	42	1	336	336
No. of voltage transducer	84	1	126	1	336	336
No. of gate drive	336	6	336	6	672	672
No. of heat sink	168	3	168	3	336	336
Estimated Cost (£)	**13366**		**16485**		**78624**	

Performance: Performance involves not only the number of switching states of different types of SMs to give the same voltage output (redundancy), but also the control complexity. The redundancy is regarded as an advantage for MMCC, which helps to charge or discharge the SM capacitors in various switching states hence guarantee minimal converter down time. Its calculation is based on the SM number and transition switching state numbers. For example, the total switching states number of a 2-level half bridge cell is 2, a 3-level h-bridge cell is 4, and could be as much as 28 for a 5-level flying capacitor cell. The control complexity is based on the number of control schemes required to meet correct operation of the UPFC application. Table IV lists the performance comparisons of the different SMs for the two UPFC configuration.

TABLE IV
PERFORMANCE COMPARISON OF PROPOSED UPFC AND DSCC-UPFC

	Single star based - UPFC				***DSCC - UPFC***	
	Shunt side	Series side	Shunt side	Series side	Shunt side	Series side
SM type	3-level h-bridge	Bridge converter	5-level flying capacitor	Bridge converter	2-level half bridge	2-level half bridge
Redundancy	336	-	1176	-	672	672
Control complexity	Cluster control				Top & Bottom arm cluster control	
	Submodule control				Submodule control	
	-				Common dc-link control	
	-				Circulating current control	

A filled radar is designed based on the above comparisons in order to display the ranking of different SM topologies and configurations for the UPFC application while 5 is the highest-ranking score and 0 is the lowest, as shown in Fig. 5. It can be seen clearly that a single star-based UPFC could be much cheaper, lighter and simpler control than the DSCC counterpart, while the latter can provide the highest redundancy due to the MMCs on its both shunt and series sides. However, a single star based UPFC assembled by the flying capacitor SMs can also provide a high enough redundancy, but only needs to cost around 20% of the DSCC-UPFC price and space.

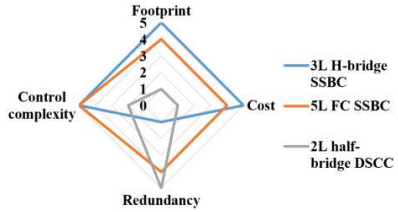

Fig. 5. Filled radar ranking of the MMCs in UPFC application

IV. CONTROL STRATEGIES

The control scheme of the proposed UPFC is divided into two main parts: control the series-connected converter ac side voltages in order to regulate the power flow from the sending to receiving ends; regulate the current flow through the shunt MMCC for voltage regulation at the sending line while maintaining all the dc capacitor voltages balanced. The overall control strategy flowchart is illustrated in Fig. 6 shown in two colours representing the two respective control parts:

- Series converter voltage control: This involves calculating the required series converter voltage V_{c2_ref} according to the reference real and reactive power commands.

- Shunt MMCC control: This requires calculating the current through shunt converter which equals the difference between the series converter current and the current through the line side current $(\overrightarrow{I_c} - \overrightarrow{I_{line}})$. This is via feedback control of the overall dc capacitor voltage. An additional dc capacitors voltage control is included to ensure the converters' voltage vector is perpendicular to their currents and thus no active power exchange between the two converters. Meantime, the MMCC is also controlled to compensate reactive current in order to regulate the PCC voltage.

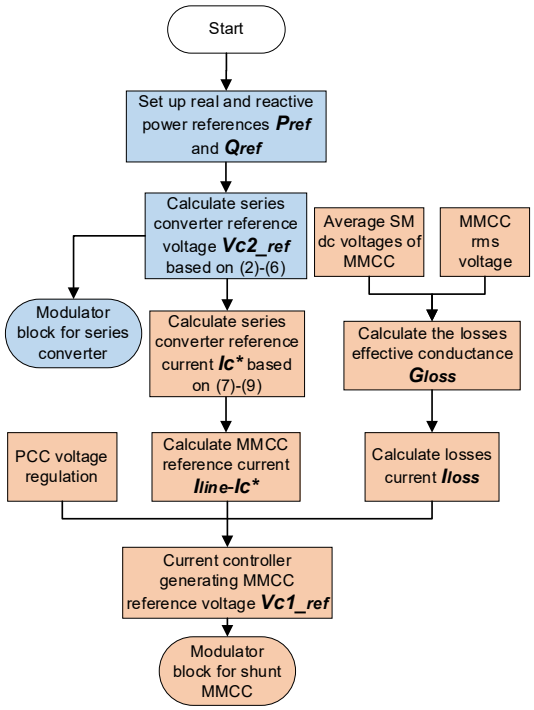

Fig. 6. Overall control strategies flowchart for the MMCC-UPFC

A. Series converter reference voltage generation

The control of transmission line power flow depends on the voltage $\overrightarrow{V_{c2s}}$ generated by the series converter and its converted value $\overrightarrow{V_{c2p}}$ at the transmission lime side. Note that all the calculations are taken the sending bus voltage as the reference. Therefore, the equation for power flow under the UPFC control can be written as

$$P_{ref} + jQ_{ref} = \overrightarrow{V_R}\overrightarrow{I_{line}}^{*} = \overrightarrow{V_R}\left(\frac{\overrightarrow{V_S} - \overrightarrow{V_R} - \overrightarrow{V_{c2p}}}{jX_L}\right)^{*}$$
$$= \left[\frac{V_R V_{c2p}\sin(\theta_R-\delta) - V_S V_R \sin\theta_R}{X_L}\right] + j\left[\frac{V_S V_R \cos\theta_R - V_R^2 - V_R V_{c2p}\cos(\theta_R-\delta)}{X_L}\right] \quad (2)$$

where P_{ref} and Q_{ref} are the user-defined transmission line real and reactive power demands. Initially, without the UPFC control, the power flow along the transmission line under the same condition is

$$P_0 + jQ_0 = \frac{-V_S V_R \sin\theta_R}{X_L} + j\frac{V_S V_R \cos\theta_R - V_R^2}{X_L} \quad (3)$$

Therefore, the 'injected' real power P_C and reactive power Q_C by the UPFC device can be calculated as

$$\begin{cases} P_C = P_{ref} - P_0 = \frac{V_R V_{c2p}\sin(\theta_R-\delta)}{X_L} \\ Q_C = Q_{ref} - Q_0 = \frac{-V_R V_{c2p}\cos(\theta_R-\delta)}{X_L} \end{cases} \quad (4)$$

From the above equation set, the required magnitude V_{c2p} and angle δ can be illustrated as

$$V_{c2p} = \frac{X_L}{V_R}\sqrt{P_C^2 + Q_C^2}$$
$$= \frac{X_L}{V_R}\sqrt{\left(P_{ref} + \frac{V_S V_R \sin\theta_R}{X_L}\right)^2 + \left(Q_{ref} - \frac{V_S V_R \cos\theta_R - V_R^2}{X_L}\right)^2} \quad (5)$$

$$\delta = \theta_R - \arctan\left(\frac{P_C}{Q_C}\right) = \theta_R - \arctan\left(\frac{P_{ref} + \frac{V_S V_R \sin\theta_R}{X_L}}{Q_{ref} - \frac{V_S V_R \cos\theta_R - V_R^2}{X_L}}\right) \quad (6)$$

The series converter reference voltage $\overrightarrow{V_{c2\_ref}}$ thus can be derived by the calculated transformer primary side magnitude V_{c2p} and its angle δ, $\overrightarrow{V_{c2\_ref}} = \frac{V_{c2p}}{\sqrt{3}}\angle(\delta - 30°)$.

B. Shunt MMCC reference current generation

Having obtained the reference voltage vector for the series converter, evaluation of MMCC-STATCOM reference current vector is needed and depending on the series converter current vector, $\overrightarrow{I_c}$. The angle of $\overrightarrow{I_c}$ is $\angle\overrightarrow{I_c} = \delta - 120°$ and the magnitude can be derived as follow:

Assuming the active power drawn by the shunt MMCC is zero and can be written as

$$P_1 = 0 = (\overrightarrow{V_s} - \overrightarrow{V_{c2s}} - \overrightarrow{V_f}) \times (\overrightarrow{I_c} - \overrightarrow{I_{line}})$$
$$= \left(\overrightarrow{V_s} - \overrightarrow{V_{c2s}} - Z_f(\overrightarrow{I_c} - \overrightarrow{I_{line}})\right) \times (\overrightarrow{I_c} - \overrightarrow{I_{line}})$$
$$= Z_f {I_c}^2 - V_s I_c \sin\delta + V_s I_{line}\cos\theta_i$$
$$+ Z_f {I_{line}}^2 - V_{c2s} I_{line}\cos(\delta - \theta_i) \quad (7)$$

Thus, I_c can be regarded as the only unknown of the above quadratic equation. Its Δ is derived as follow.

$$\Delta = (V_s \sin\delta)^2 - 4Z_f(V_s I_{line}\cos\theta_i + Z_f {I_{line}}^2$$
$$- V_{c2s} I_{line}\cos(\delta - \theta_i)) \quad (8)$$

This equation can only be solved when $\Delta \geq 0$, otherwise there is no solution of I_c, which means the UPFC cannot work under that condition, thus

$$I_c = \frac{V_s \sin\delta \pm \sqrt{\Delta}}{2Z_f} \quad (9)$$

So, $\overrightarrow{I_c} = \frac{V_s \sin\delta \pm \sqrt{\Delta}}{2Z_f}\angle\delta - 90°$ and subsequently the shunt MMCC reference current can be derived through $(\overrightarrow{I_c} - \overrightarrow{I_{line}})$.

However, in practice a certain amount of real power is required to compensate the converter losses, hence the MMCC voltage and current cannot be exactly in quadrature since the MMCC current must have a small in-phase element for loss compensation. This element is evaluated through an additional overall dc capacitor voltage control loop as follows.

Evaluation of the real power loss in the MMCC is performed by measuring all SM dc capacitor voltages and calculating their average value. By comparing this average voltage with its

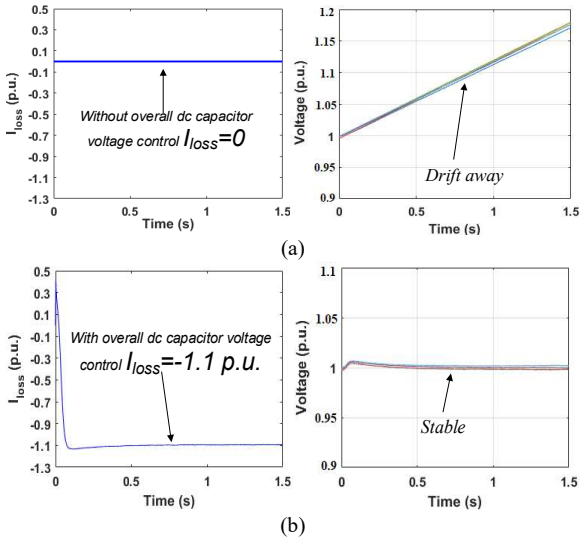

Fig. 7. The I_{loss} current (left) and MMCC dc capacitor voltages (right) (a) without and (b) with overall dc capacitor voltage control

required value and applying the P+I control, the value of real power loss, P_{loss}, is obtained. Dividing this by the MMCC voltage (rms) squared leads to conductance G_{loss}. Multiplying G_{loss} with voltage gives the current I_{loss} required for compensating the loss. This result can be added to the $(\overrightarrow{I_c} - \overrightarrow{I_{line}})$ to generate the MMCC reference current I_{ref}. Fig. 7 shows the resultant average dc capacitor voltage without and with the additional real power compensation current. It can be seen that the dc capacitors voltage can be maintained at its nominal value (Fig.7 (b)) when I_{loss} is added otherwise it drifts away when I_{loss} is zero (Fig.7 (a)).

With the shunt MMCC reference current obtained, a predictive current controller [26] is applied to generate the reference voltage V_{c1_ref} as this control scheme has the benefits of fast dynamic response and high computational efficiency. The vector model for MMCC voltage evaluation is given by

$$\overrightarrow{V_s} - \overrightarrow{V_{c1}} = L_f \frac{d\vec{\imath}}{dt} + R_f \vec{\imath} \tag{10}$$

Digital implementation with a small sampling period (T_s) leads to $\frac{d\vec{\imath}}{dt}$ expressed by

$$\frac{d\vec{\imath}}{dt} = \frac{\Delta\vec{\imath}}{T_s} = \frac{\vec{\imath}(k+1) - \vec{\imath}(k)}{T_s} \tag{11}$$

where $\vec{\imath}(k)$ is the measured current at time instant k, and the current at the next sampling interval $\vec{\imath}(k+1)$ is set as the current reference value $\overrightarrow{\imath_{ref}}(k)$. Substituting (11) into (10) and re-arranging the equation, the required reference voltage at the next sampling period can be derived as

$$\overrightarrow{V_{c1\_ref}}(k) = \overrightarrow{V_s}(k) - \left[\frac{L_f}{T_s}\right]\overrightarrow{\imath_{ref}}(k) + \left[\frac{L_f}{T_s} - R_f\right]\vec{\imath}(k) \tag{12}$$

C. Carrier Permutation Phase Shift- Pulse Width Modulation for MMCC

For MMCC switching signal generation the well-known Phase-Shift Pulse Width Modulation (PS-PWM) scheme is applied. The advantages of this scheme are giving lower THD with a relatively low switching frequency and maintaining natural voltage balance to the SM capacitors. However, if the FCC submodule is adopted, the regular PS-PWM schemes cannot always ensure the balance of inner flying capacitor voltage particularly when the converter reference voltage is distorted [27]. For example, Fig. 8 shows the results of a FCC-MMCC phase A reference voltage compared with four carrier waveforms. The slight distortion in reference voltage causes imbalance in the SM capacitors' charging and discharging currents, and hence the total net charge transferred over one cycle is non-zero even during steady state. Consequently, the FCC SM flying capacitor voltages in each phase drift away from the nominal value as shown in Fig. 9.

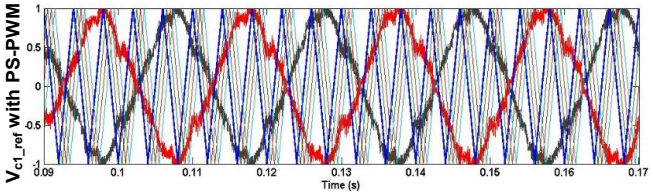

Fig. 8. Voltage reference signal for FCC-MMCC with conventional PS-PWM

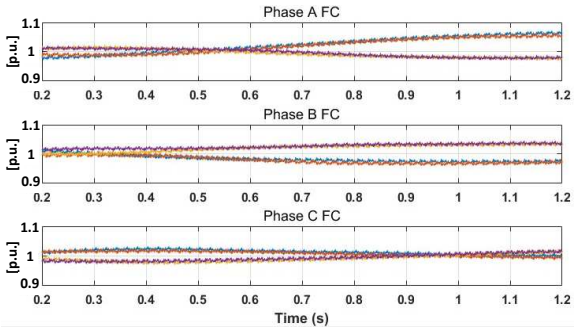

Fig. 9. SM FCC voltages with conventional PS-PWM

This paper adopts a carrier permutation (CP) PS-PWM scheme [27] to prevent the inner capacitor voltage drifts. The method uses multiple triangular carrier waveforms, but instead of applying each of them in a fixed sequence cycle by cycle they are cyclically permuted one position forward at the end of each fundamental cycle. Naturally with four carrier waves in this example a complete permutation cycle takes four fundamental cycles or 0.08 s, as shown in Fig. 10. This enables the charging and discharging current through the SM capacitors to vary from cycle to cycle according to the reference voltage pattern, and hence greatly reduces the voltage drift. As shown in Fig. 11, the voltages are all stable and around 1 p.u.. This validates that the CP PS-PWM scheme can effectively prevent the inner flying capacitor drifting away from the nominal value when the voltage reference is distorted.

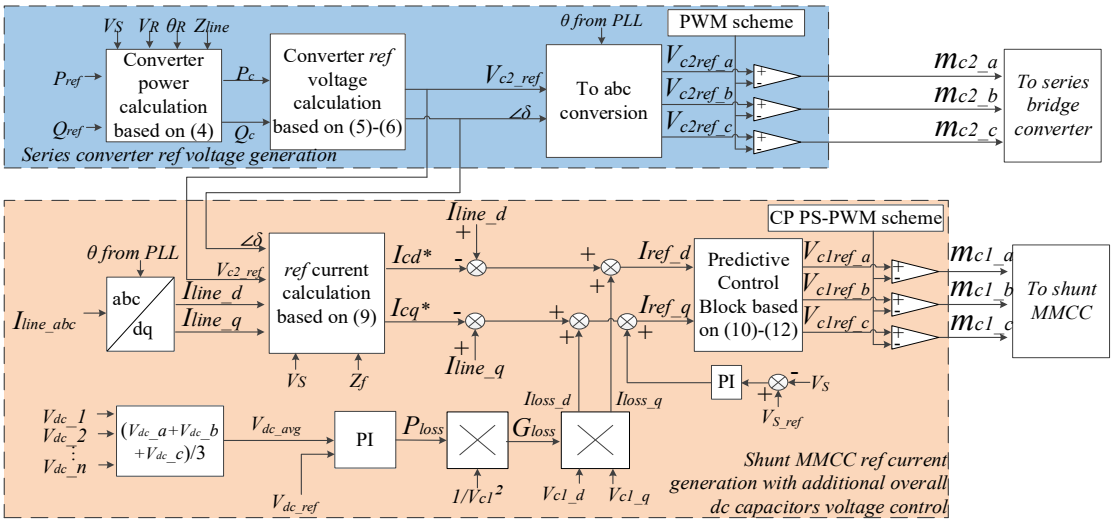

Fig. 12. MMCC-UPFC control block diagram.

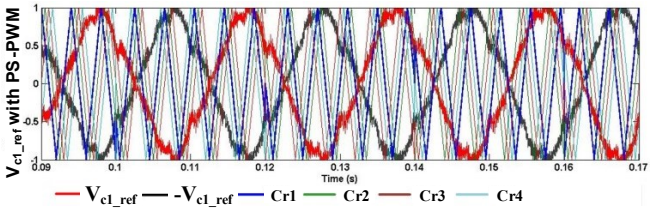

Fig. 10. Voltage reference signal for FCC-MMCC with CP PS-PWM

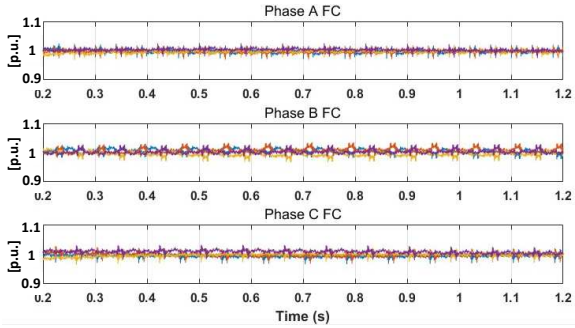

Fig. 11. SM FCC voltages with CP PS-PWM

The overall single star MMCC-UPFC control scheme is shown in Fig. 12, which comprises two essential parts: the series converter reference voltage generation and the shunt MMCC reference current generation with additional overall dc capacitors voltage control.

V. Simulation Results

To validate the effectiveness of the proposed MMCC-UPFC device shown in Fig. 2 and the corresponding control schemes shown in Fig. 12, the system is simulated through SIMULINK/MATLAB, as presented in Fig. 13. Its parameters are listed in Table V: the three-phase voltage rating at the sending end is 11 kV, 50 Hz; the MMCC total dc voltage rating is 12.8 kV containing 32 FCC SMs in each phase, while the dc capacitor voltage per SM is 400 V and the floating flying capacitors are rated at 200 V. The series converter contains one dc capacitor and its voltage rating is 600 V.

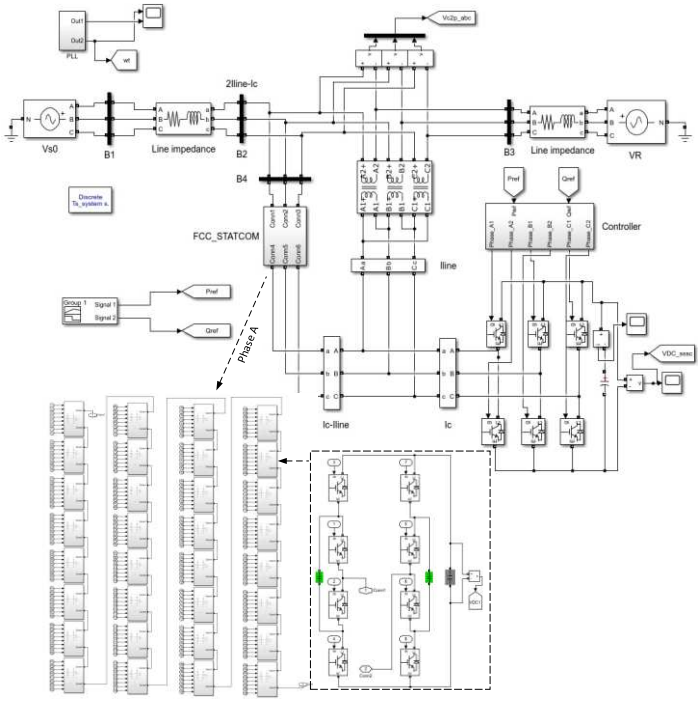

Fig. 13. Simulink program setup screenshot

For testing MMCC-UPFC's ability in power flow control, the receiving end voltage is set to 10.45 kV and phase angle -10° initially without MMCC-UPFC, so the real and reactive power of the transmission line are P_0 =0.1141 p.u. and Q_0=0.0229 p.u. respectively. At 0.2 s, the MMCC-UPFC is switched on and the command P_{ref} and Q_{ref} are 0.6 p.u. and -0.1 p.u. As shown in Fig. 14, under UPFC control, the real and reactive powers transmitted to the receiving bus follow the command values closely. Similarly at 0.3 s the real power drops to 0.2 p.u. according to the set reference values, while the reactive power is controlled to drop to 0, thus the UPFC is able to achieve unity power factor control. Clearly the MMCC-UPFC device can control both real and reactive powers of the transmission line to the required values precisely and fast.

TABLE V
SYSTEM PARAMETERS

Components		Rating
Source Side	3-Phase source voltage V_{s0}	11 kV
	Fundamental frequency f_0	50 Hz
Transmission line	Transmission line inductance X_L	8.4 mH
UPFC shunt MMCC side	MMCC switching frequency f_{c1}	250 Hz
	Low-pass filter	0.5 Ω, 1.0 mH
	SM numbers per phase	32
	SM dc capacitor C_{dc1_n}	1120 µF
	SM flying capacitor C_{fc}	560 µF
	Nominal SM dc voltage V_{dc1_n}	400 V
UPFC series bridge converter side	Series transformer turn ratio $n_1: n_2$	10:1
	Series converter dc capacitor C_{dc2}	560 µF
	Nominal series converter dc voltage V_{dc2}	600 V
	Bridge converter switching frequency f_{c2}	8 kHz

Fig. 15 shows the transmission line 3-phase voltages with their corresponding currents, UPFC shunt and series part respectively. As expected, the MMCC controls its current (Fig. 15(b)) to be equal to the difference between transmission line current (Fig. 15(a)) and series converter's current (Fig. 15(c)), which is $(\vec{I_c} - \vec{I_l})$. At 0.3 s, the transmission line current reduced to around 0.3 p.u. and become in phase with its 3-phase voltage due to the changing of real and reactive power command values, consequently the series bridge converter current decreases while the shunt MMCC current remains stable, which indicates that the control schemes of both shunt and series converters are chained well and responding fast. Meantime, Fig. 15(a) also illustrates that the PCC voltage V_S is regulated at 1 p.u.; Fig. 15(b) and (c) show that at the steady state the ac voltages of the two converters are in quadrature with their currents hence no active power exchange in both converters, while the shunt MMCC is inductive and series converter is capacitive. Therefore, the MMCC module dc capacitor voltages and the series converter voltage are well maintained at their nominal value 1.0 p.u. respectively, as shown in Fig. 16. Finally, the 3-phase MMCC terminal multilevel voltage waveform is shown in Fig. 17 with a peak value around 1.136 p.u.

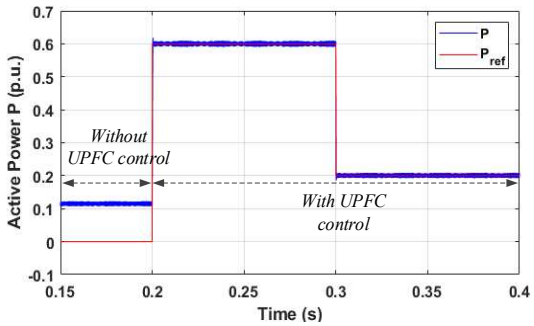

(a) Real power P_{ref}

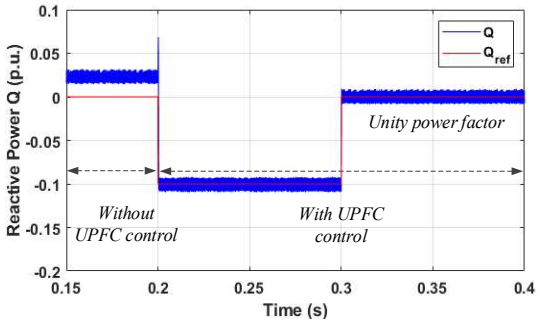

(b) Reactive power Q_{ref}

Fig. 14. Transmission line power flow diagrams with reference waveforms

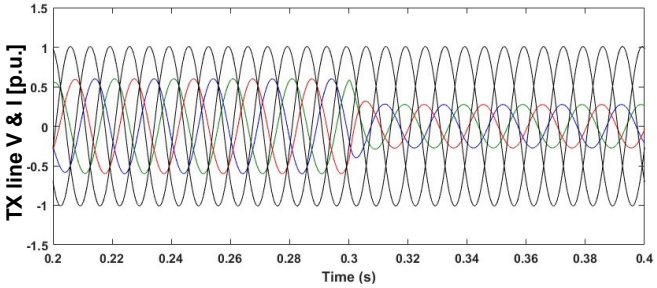

(a) Transmission line PCC 3-phase voltage (black) and current

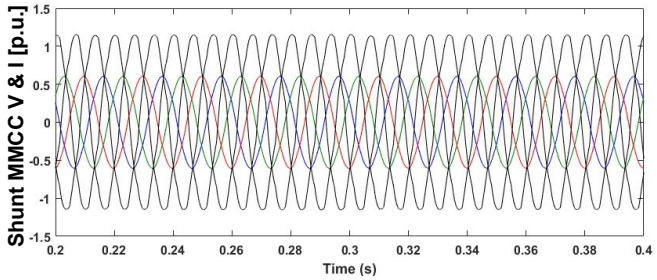

(b) Shunt MMCC 3-phase voltage (black) and current

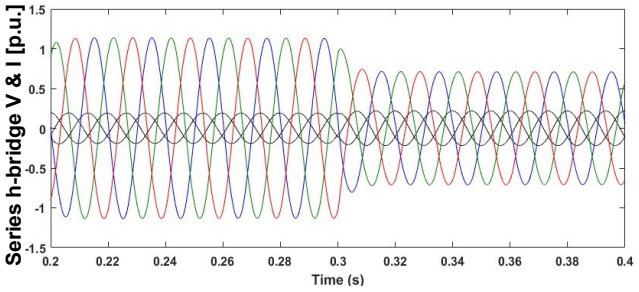

(c) Series bridge converter 3-phase voltage (black) and current

Fig. 15. MMCC-UPFC system simulated 3-phase voltages and currents

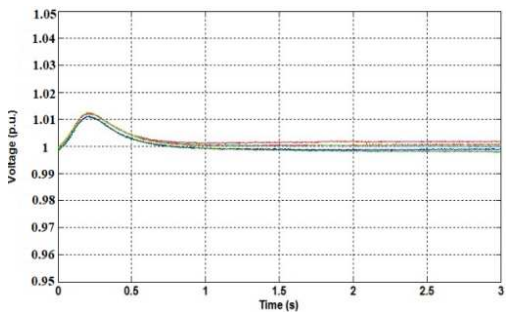

(a) Shunt MMCC

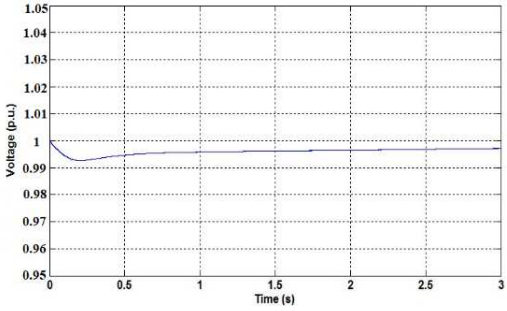

(b) Series bridge converter

Fig. 16. Converter dc capacitors voltage

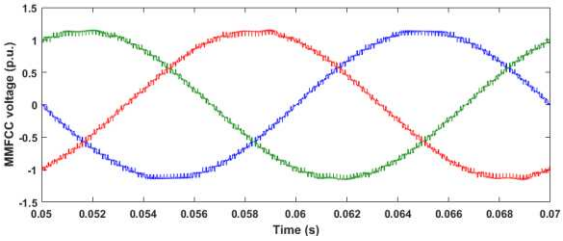

Fig. 17. 3-phase MMCC multilevel voltage waveform

VI. MMCC-UPFC OPERATING RANGE ASSESSMENT

According to the above results, it can be seen that the novel device is able to operate as an UPFC for controlling the grid real and reactive powers. However, it is also important to study its operating margins, which are limited by two essential factors: (a) the series bridge converter and (b) the shunt MMCC operating margins. For (b), it only works when the calculated $\Delta \geq 0$ hence the margin is decided by Δ. The following study investigates (a) the series bridge converter operating margin. Finally, combining both calculated margins together gives the operating range of the MMCC-UPFC.

According to the phasor diagram shown in Fig. 3(b), the equations below can be derived as

$$\overrightarrow{V_D} = \overrightarrow{V_s} - \overrightarrow{V_R} = \overrightarrow{V_{c2p}} + L_{line}\frac{d\overrightarrow{i_{line}}}{dt} \tag{13}$$

where $\overrightarrow{V_D}$ is the voltage potential difference between the sending and receiving ends.Taking $\overrightarrow{V_s}$ as the reference vector in synchronous reference frame, the above equation can be re-written in *d-q* form as

$$\begin{cases} V_{Dd} = V_s - V_R\cos\theta_R \\ V_{Dq} = V_R\sin\theta_R \end{cases} \tag{14}$$

$$\theta_D = \tan^{-1}\frac{V_R\sin\theta_R}{V_s - V_R\cos\theta_R} \tag{15}$$

Having UPFC connected into the transmission line the relationship between its series bridge converter terminal voltage V_{c2p}, transmission line current i_{line} and the line impedance can be illustrated as

$$\begin{cases} V_{Dd} = V_{c2p}\cos\delta - X_L i_{line}\sin\theta_i \\ V_{Dq} = V_{c2p}\sin\delta + X_L i_{line}\cos\theta_i \end{cases} \tag{16}$$

The current of the equation (16) can be further derived as

$$\begin{cases} i_{line}\cos\theta_i = i_{line\_d} = \frac{V_{Rq} - V_{c2p\_q}}{X_L} \\ i_{line}\sin\theta_i = i_{line\_q} = \frac{-V_s + V_{Rd} + V_{c2p\_d}}{X_L} \end{cases} \tag{17}$$

Thus the operating margin of the UPFC series bridge converter is derived as

$$P_{ref} = -\frac{3}{2}\times\left(V_{sd}i_{line\_d} + V_{sq}i_{line\_q}\right) = -\frac{3}{2}V_s i_{line\_d} = \frac{3V_s(V_{Rq} - V_{c2pq})}{2X_L} \tag{18}$$

$$Q_{ref} = -\frac{3}{2}\times\left(V_{sd}i_{line\_q} - V_{sq}i_{line\_d}\right) = -\frac{3}{2}V_s i_{line\_q} = \frac{3V_s(-V_s + V_{Rd} + V_{c2pd})}{2X_L} \tag{19}$$

Assuming the transmission line length is 50km with reactance of 0.053 Ω/km at 50 Hz according to the UK power networks 11 kV line parameters given in [28], taking 2.2 MVA as base power and the UPFC capacity is 3.2 MVA, combining the above derivation with the shunt MMCC margin ($\Delta \geq 0$) the UPFC operating ranges now can be illustrated graphically via 3-D plots, together with the 2-D plots of (δ, P_{ref}) and (δ, Q_{ref}) as shown in Fig. 18 and Fig. 19. The *X*-axis is V_{c2p} magnitude in p.u., *Y*-axis is phase angle $\angle\delta$ and *Z*-axis is either P_{ref} or Q_{ref} in p.u.. The 3-D diagrams illustrate clearly that the maximum real power the UPFC able to control is -0.35 p.u.$\leq P_{ref} \leq$0.69 p.u. The reactive power is in the range -0.58 p.u.$\leq Q_{ref} \leq$0.45 p.u, while without UPFC the original real and reactive power between the buses are P_0=0.1141 p.u. and Q_0=0.0229 p.u. respectively.

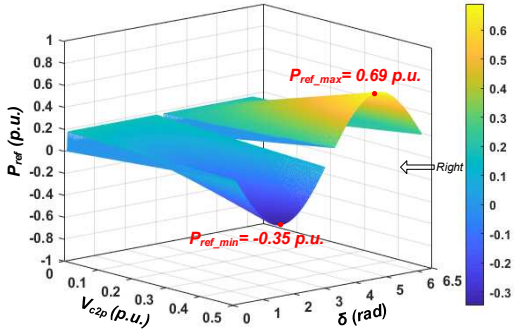

(a)

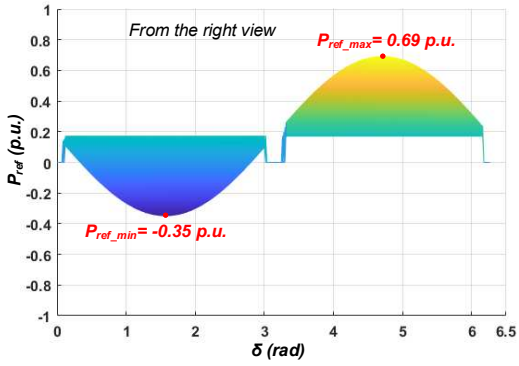

(b)

Fig. 18. MMCC-UPFC real power operating range (a) 3-D diagram (b) view from the right

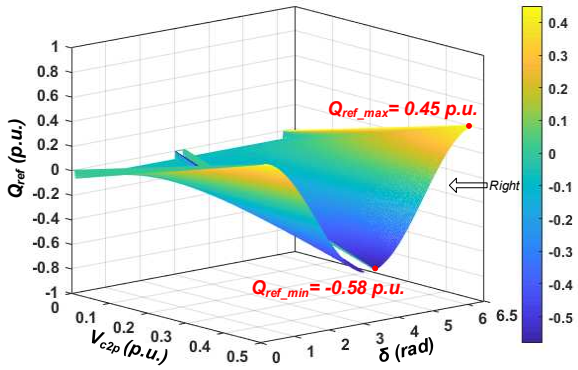

(a)

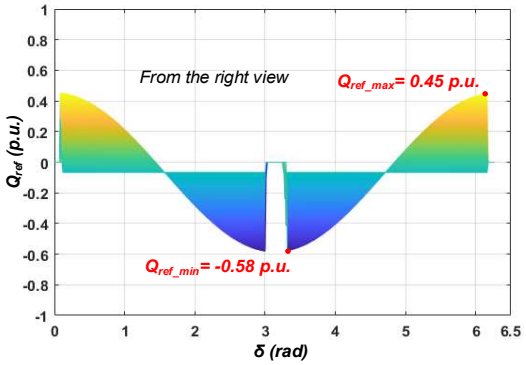

(b)

Fig. 19. MMCC-UPFC reactive power operating range (a) 3-D diagram (b) view from the right

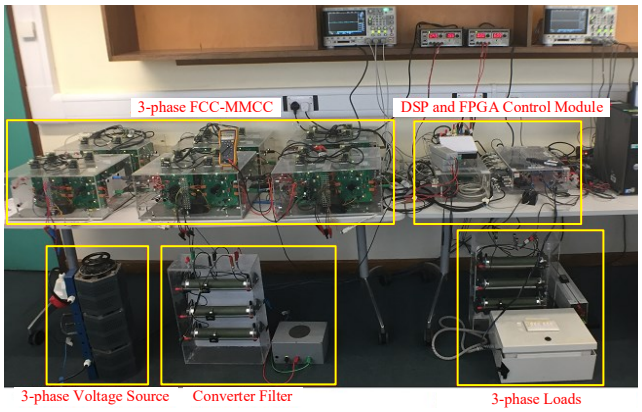

Fig. 20. FCC-MMCC STATCOM laboratory set-up prototype

TABLE VI
FCC-MMCC STATCOM KEY COMPONENTS PARAMETERS

Components	Value
Source end voltage V_{s0}	110 V
Distribution Line	R_{line}= 0.2 Ω; L_{line}= 3 mH
R+L Load	R_l = 20 Ω; L_l = 48 mH
Converter Filter	R_c = 1.59 Ω; L_c = 2 mH
Sub-module DC capacitor	C_{DC}= 1.12 mF
DC voltage V_{DC} in each sub-module	100 V
Switching frequency f_s	1 kHZ

Construction of an experimental MMCC-UPFC for validating the proposed control scheme is in hand. Fig. 20 shows a photo of the already built FCC-MMCC STATCOM. The series converter for a complete UPFC is yet to be connected. The key component values for the STATCOM is given in Table VI. This STATCOM has been applied to compensate reactive current of an AC network. The measured current and voltage waveforms prior and post compensation are shown in Fig. 21 which demonstrate desired performance for reactive power compensation.

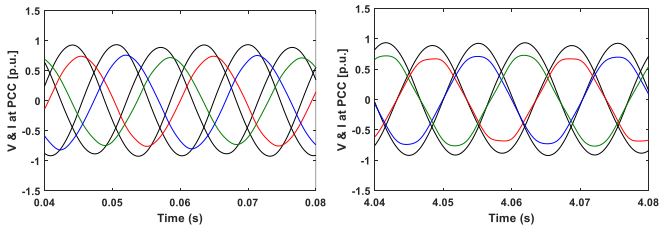

(a) (b)

Fig. 21 FCC-MMCC STATCOM reactive power compensation voltage and current waveforms (a) before compensation (b) after compensation

VII. CONCLUSION

A single-star modular multilevel cascaded converter-unified power flow controller (MMCC-UPFC) has been proposed to provide highly flexible power flow control in the power transmission system. Compared with the double star chopper cell based-UPFC, this device has been estimated to only cost around 20% in both price and space but provides similar redundancy and simpler control. The operating principle of this novel device was explained, together with control schemes for the series bridge converter voltage generation and the shunt MMCC current regulation were illustrated. Simulation results have shown that the device can react precisely to control the transmission line power to the required level. The UPFC's ability to increase the line's power transfer margin and its operating range were also analysed and illustrated via the 3-D plots, showing that it can compensate real power in the range of -0.35 p.u. $\leq P_{ref} \leq$ 0.69 p.u. The reactive power compensation range is -0.58 p.u.$\leq Q_{ref} \leq$ 0.45 p.u.

REFERENCES

[1] N. G. Hingorani and L. Gyugyi, "FACTS concept and general system considerations," *Understanding FACTS: Concepts and Technology of Flexible AC Transmission Systems,* pp. 1-35, 2000.

[2] L. Gyugyi, C. Schauder, S. Williams, T. Rietman, D. Torgerson, and A. Edris, "The unified power flow controller: A new approach to power transmission control," *IEEE Trans. Power Delivery,* vol. 10, no. 2, pp. 1085-1097, 1995.

[3] A. Nabavi-Niaki and M. R. Iravani, "Steady-state and dynamic models of unified power flow controller (UPFC) for power system studies," *IEEE Trans. Power Syst.,* vol. 11, no. 4, pp. 1937-1943, 1996.

[4] S. Yang, Y. Liu, X. Wang, D. Gunasekaran, U. Karki, and F. Z. Peng, "Modulation and control of transformerless UPFC," *IEEE Trans. Power Electron.,* vol. 31, no. 2, pp. 1050-1063, 2016.

[5] J. Monteiro, J. F. Silva, S. Pinto, and J. Palma, "Matrix converter-based unified power-flow controllers: Advanced direct power control method," *IEEE Trans. Power Delivery,* vol. 26, no. 1, pp. 420-430, 2011.

[6] J. Monteiro, J. F. Silva, S. F. Pinto, and J. Palma, "Linear and sliding-mode control design for matrix converter-based unified power flow controllers," *IEEE Trans. Power Electron.,* vol. 29, no. 7, pp. 3357-3367, 2014.

[7] Z. Yuan, S. W. de Haan, J. B. Ferreira, and D. Cvoric, "A FACTS device: Distributed power-flow controller (DPFC)," *IEEE Trans. Power Electron,* vol. 25, no. 10, pp. 2564-2572, 2010.

[8] F. Z. Peng and J.-S. Lai, "Multilevel cascade voltage source inverter with separate dc sources," Lockheed Martin Energy Syst Inc, 1997.

[9] S. Debnath, J. Qin, B. Bahrani, M. Saeedifard, and P. Barbosa, "Operation, control, and applications of the modular multilevel converter: A review," *IEEE Trans. Power Electron.,* vol. 30, no. 1, pp. 37-53, 2014.
[10] J. Tang *et al.*, "Research on AC transmission line fault ride-through control strategy of MMC-based unified power flow controller," *The Journal of Engineering,* vol. 2017, no. 13, pp. 1580-1583, 2017.
[11] H. Cai, L. Yang, H. Wang, P. Song, and Z. Xu, "Application of Unified Power Flow Controller (UPFC) in Jiangsu power system," in *2017 IEEE Power & Energy Society General Meeting*, 16-20 July 2017, pp. 1-5.
[12] P. Li, Y. Wang, C. Feng, and J. Lin, "Application of MMC-UPFC in the 500 kV power grid of Suzhou," *The Journal of Engineering,* vol. 2017, no. 13, pp. 2514-2518, 2017.
[13] Y. Cui *et al.*, "Analysis of application effect of 220 kV UPFC demonstration project in Shanghai grid," *The Journal of Engineering,* vol. 2019, no. 16, pp. 758-762, 2019.
[14] A. M. Vural and E. N. Wirsiy, "Three-phase modular multilevel converter based unified power flow controller," *Engineering Science and Technology, an International Journal,* vol. 23, no. 2, pp. 299-306, 2020
[15] Y. Yuan, P. Li, X. Kong, J. Liu, Q. Li, and Y. Wang, "Harmonic influence analysis of unified power flow controller based on modular multilevel converter," *Journal of Modern Power Systems and Clean Energy,* vol. 4, no. 1, pp. 10-18, 2016.
[16] J. Yang, P. Song, Z. Xu, H. Xiao, H. Cai, and Z. Xie, "Small-signal model of vector current-controlled MMC-UPFC," *IET Generation, Transmission & Distribution,* vol. 13, no. 18, pp. 4180-4189, 2019.
[17] Q. Hao, J. Man, F. Gao, and M. Guan, "Voltage Limit Control of Modular Multilevel Converter Based Unified Power Flow Controller Under Unbalanced Grid Conditions," *IEEE Trans. Power Delivery,* vol. 33, no. 3, pp. 1319-1327, 2018.
[18] Q. Yang *et al.*, "Model predictive control of MMC-UPFC under unbalanced grid conditions," *Int. J. Electr. Power Energy Syst.,* vol. 117, p. 105637, 2020
[19] H. Akagi, "Classification, terminology, and application of the modular multilevel cascade converter (MMCC)," *IEEE Trans. Power Electron,* vol. 26, no. 11, pp. 3119-3130, 2011.
[20] F. Qin, F. Gao, T. Xu, D. Niu, and Z. Ma, "A Unified Power Flow Controller With Nine-Arm Modular Multilevel Converter," in *2018 IEEE Energy Conversion Congress and Exposition (ECCE)*, 23-27 Sept. 2018, pp. 2581-2587.
[21] N. MacLeod, C. Davidson, N. Kirby, and U. Stafford, "A multi-level topology for Voltage Source Converter (VSC) HVDC transmission projects," in *EPRI HVDC/FACTS Conference, Palo Alto, California, USA*, 2010.
[22] O. Oghorada, "Modular multilevel cascaded flying capacitor STATCOM for balanced and unbalanced load compensation," University of Leeds, 2017.
[23] A. Grid, "HVDC-VSC: transmission technology of the future," *Alstom Grid,* vol. 1, pp. 13-17, 2011.
[24] https://www.farnell.com/.
[25] T. IEC, "60815-1--2008," *Selection and dimensioning of high-voltage insulators intended for use in polluted conditions-Part,* vol. 1.
[26] L. Zhang, M. J. Waite, and B. Chong, "Three-phase four-leg flying-capacitor multi-level inverter-based active power filter for unbalanced current operation," *IET Power Electronics,* vol. 6, no. 1, pp. 153-163, 2013.
[27] H. Huang, O. K. Oghorada, L. Zhang, and B. Chong, "Active harmonic current elimination and reactive power compensation using modular multilevel cascaded converter," in *19th European Conference on Power Electronics and Applications (EPE'17 ECCE Europe)*, 2017: IEEE, pp. P. 1-P10.
[28] B. Fox *et al.*, *Wind power integration: connection and system operational aspects*. IET, 2007.